Organic Semiconductors

Deutsche Ausgabe: DOI: 10.1002/ange.201504576
Internationale Ausgabe: DOI: 10.1002/anie.201504576

Charge and Spin Transport in an Organic Molecular Square

Yilei Wu, Siva Krishna Mohan Nalluri, Ryan M. Young, Matthew D. Krzyaniak, Eric A. Margulies, J. Fraser Stoddart, and Michael R. Wasielewski**

Abstract: *Understanding electronic communication among multiple chromophoric and redox units requires construction of well-defined molecular architectures. Herein, we report the modular synthesis of a shape-persistent chiral organic square composed of four naphthalene-1,8:4,5-bis(dicarboximide) (NDI) sides and four trans-1,2-cyclohexanediamine corners. Single crystal X-ray diffraction reveals some distortion of the cyclohexane chair conformation in the solid state. Analysis of the packing of the molecular squares reveals the formation of highly ordered, one-dimensional tubular superstructures, held together by means of multiple [C−H···O=C] hydrogen-bonding interactions. Steady-state and time-resolved electronic spectroscopies show strong excited-state interactions in both the singlet and triplet manifolds. Electron paramagnetic resonance (EPR) and electron-nuclear double resonance (ENDOR) spectroscopies on the monoreduced state reveal electron sharing between all four NDI subunits comprising the molecular square.*

Construction of ordered organic molecular architectures capable of delocalization or fast hopping of charge among neighboring units is a prerequisite for organic electronics and photovoltaics.[1] Extensive experimental effort has been made by us[2] and others[3] to develop multichromophoric systems capable of significant charge delocalization. While hole hopping between up to seven porphyrins has been observed[3a] in multiporphyrinic assemblies by using electron paramagnetic resonance (EPR) spectroscopy, the direct observation of electron sharing over more than three aromatic units is unprecedented.

Naphthalene-1,8:4,5-bis(dicarboximide) (NDI) (Scheme 1) and its derivatives[4] have attracted considerable attention as n-type electroactive materials in organic field-effect transistors[5] (OFETs) and photovoltaics[6] (OPVs). NDIs can also be used 1) as versatile units for molecular recognition,[7] 2) as electron acceptors for photoinduced charge- and energy-transfer studies,[8] and 3) as platforms for organocatalysis.[9] Recently, we have reported two pairs of enantiomerically pure cyclic oligomers of NDI—namely, (−)- and (+)-**3NDI** (trimer)[10a] and (−)- and (+)-**2NDI** (dimer)[10b]—and investigated their electronic and magnetic properties. The π systems of these units in the macrocycles interact strongly. Their one-electron chemical reduction results in stable radical anions in which the electron is shared fully between the NDI units. In the quest to advance our understanding of how molecular geometry affects through-space orbital overlap and electron sharing, we have designed and developed a modular synthesis (Scheme 1) of a pair of chiral shape-persistent[11] macrocyclic diimide squares[12]—namely, (−) and (+)-**4NDI**. In the present work, we have investigated the photophysical and magnetic properties of **4NDI** and compared them with those of the smaller macrocycles—namely, **2NDI** and **3NDI**—as well as with a monomeric reference compound **Ref-NDI. 4NDI** has has been characterized by 1) high-resolution mass spectrometry in the gas phase, 2) 1D and 2D NMR spectroscopies, as well as 3) optical spectroscopies in the solution phase, and 4) single-crystal X-ray diffraction in the solid state. Furthermore, we show by means of electronic spectroscopy and cyclic voltammetry how the excitonic and electronic interactions between neighboring chromophores are strongly dependent on their relative orientations and center-to-center distances. We have employed ultrafast transient absorption spectroscopy to reveal how the excited-state dynamics in these non-conjugated multichromophoric architectures also depends on conformation. Finally, we established, by means of electron paramagnetic resonance (EPR) and electron-nuclear double resonance (ENDOR) spectroscopies, that electron sharing occurs between all four NDI units in monoreduced $[\mathbf{4NDI}]^{\cdot-}$, a remarkable result given the small interchromophoric overlap of the π orbitals enforced by the square geometry.

4NDI was prepared in an overall yield of 8% by stepwise condensations, starting from naphthalenetetracarboxylic dianhydride and (*R*,*R*)-*trans*-1,2-cyclohexanediamine in DMF at 130 °C (Scheme 1). This stepwise route[13] facilitates purification and leads to an improved yield of **4NDI** compared to a one-pot approach (ca. 1% yield; see the Supporting Information for further details). The NDI square **4NDI** was identified 1) by atmospheric-pressure photoionization coupled to high-resolution mass spectrometry (APPI-HRMS; Figure S1 in the Supporting Information) and 2) by NMR spectroscopy. The ^{1}H NMR spectrum (Figure S2) exhibits the characteristic resonances from the protons of the NDI unit in the region, $\delta = 8$–9 ppm, and the aliphatic protons of the linker cyclohexane chains at higher field, $\delta = 1.5$–6.5 ppm. The observation of only a single set of resonances in the ^{13}C NMR spectrum (Figure S3) of **4NDI** is indicative of high symmetry (point group D_4) and restricted conformational mobility. A comparison of the ^{1}H (Figure 1) and ^{13}C (Fig-

[*] Y. Wu, Dr. S. K. M. Nalluri, Prof. R. M. Young, Dr. M. D. Krzyaniak, E. A. Margulies, Prof. J. F. Stoddart, Prof. M. R. Wasielewski
Argonne-Northwestern Solar Energy Research (ANSER) Center and Center for the Chemistry of Integrated Systems (CCIS)
Department of Chemistry, Northwestern University
2145 Sheridan Road, Evanston, IL 60208-3113 (USA)
E-mail: stoddart@northwestern.edu
m-wasielewski@northwestern.edu

Supporting information for this article (including experimental details on synthesis, mass spectrometry, ^{1}H and ^{13}C NMR, steady-state and time-resolved electronic spectroscopy, electrochemical measurements, EPR and ENDOR spectroscopy) is available on the WWW under http://dx.doi.org/10.1002/anie.201504576.

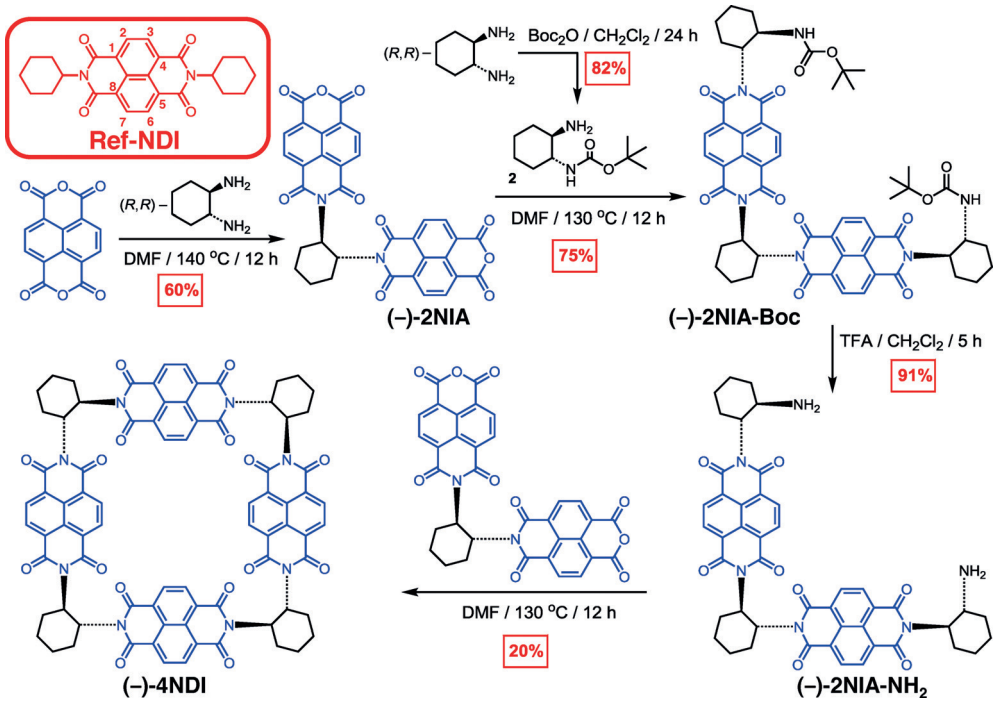

Scheme 1. Stepwise preparation of (−)-**4NDI** from (*R*,*R*)-*trans*-1,2-cyclohexanediamine and naphthalenetetracarboxylic dianhydride. The enantiomer (+)-**2NDI** was obtained in a similar fashion from (*S*,*S*)-*trans*-1,2-cyclohexanediamine.

ure S4) NMR spectra of this series of macrocyclic diimides shows a downfield shift of the two diastereotopic proton resonances (from 8.26 and 8.23 ppm for **2NDI**, to 8.49 and 8.47 ppm for **3NDI**, and 8.60 and 8.57 ppm for **4NDI**), which are resolved into separate doublets ($^3J_{AB} = 7.5$ for **2NDI** and $^3J_{AB} = 7.7$ for **3NDI** and **4NDI**) because of the restricted rotation around the C–N bonds and the rigidity of cyclohexane ring (Table 1).[14]

In order to elucidate further structural details (i.e., constitution, molecular shape, bond lengths, bond angles), we performed an X-ray diffraction analysis[15] (Figure 2) on single crystals, obtained by slow vapor diffusion of *n*-hexane into a 1.0 mM solution of **4NDI** in $CHCl_3$ at room temperature. The chiral (+)-**4NDI** is made (Figure 2a) from four NDI faces linked together by four (*S*,*S*)-*trans*-1,2-cyclohexanediamine corners, resulting in a rigid square-shaped macrocycle with a face-to-face distance of 11 Å and an easily accessible interior cavity.[16] A careful analysis of the X-ray diffraction data of all three NDI macrocycles reveals the ring puckering of the cyclohexane bridging units from their ideal chair conformations, a situation which is supported by NMR spectroscopy. The values of selected bond length, bond angles, and torsional angles show (Figure S7) an increase of the ∡N1-C1-C2 (and ∡C1-C2-N2) bond angles from 112° in a strain-free cyclohexane[17] with vicinal diimide substituents in the equatorial positions up to 116° in **2NDI** and **4NDI**, and a decrease of ∡N1-C1-C2-N2 gauche torsional angles from an unstrained value of 54°[17] down to 48° in **3NDI**, 45° in **4NDI**, and 37° in **2NDI**. The average torsional angle magnitudes within the cyclohexane rings are 59° in **2NDI**, 58° in **3NDI**, and 57° in **4NDI**. These values are significantly higher than that (54.9°) reported[16] for a cyclohexane ring in an unstrained chair conformation, indicating significant ring puckering. The strain energy enforced by the macrocyclization is also localized on the NDI units, forcing their aromatic planes to be bent with a displacement of 0.4 Å in **2NDI** and 0.1 Å in both **3NDI** and **4NDI**.[18] The relative total strain energy can be estimated by comparing the computed (B3LYP/6-31G**) ground-state energies (Figure S8), which show that **3NDI** is the least strained compound among the three NDI polygons. In the single-crystal superstructure of **4NDI**, two crystallographically distinct NDI squares are observed (Figure 2b) to be held together by means of multiple intermolecular [C–H···O=C] hydrogen bonds between the carbonyl oxygen atoms and the NDI protons ($3.0\ \text{Å} < d_{C\cdots O=C} = 3.5\ \text{Å}$, $2.1\ \text{Å} < d_{C-H\cdots O=C} < 2.7\ \text{Å}$, $138° < \measuredangle_{C-H\cdots O} < 152°$) interactions. These supramolecular dimers, which are composed of two **4NDI** molecules with a twist angle of around 45°, stack along the *c*-axis (Figure 2b and Figure S6) to form infinite coaxial channels filled with disordered solvent molecules (Figure 2c). Bundles of these sheath-like organic nanotubes are then tightly packed to form well-ordered arrays that constitute the single crystal (Figure S6b).

The optical properties were investigated by UV/Vis absorption spectroscopy (Figure 3a). These spectra show an intensity reversal for the 0←0 and 0←1 vibronic bands of the $S_1 \leftarrow S_0$ electronic transition (with maxima at 360 and 380 nm,

Table 1: ^{1}H and ^{13}C chemical shifts obtained from the ^{1}H and ^{13}C NMR spectra recorded in $CDCl_3$ at 298 K, for the cyclohexane ring protons and carbon atoms in **2NDI**, **3NDI** and **4NDI** in comparison with the resonances for the analogous protons and carbons in **2NIA**.

	δ [ppm]								
	H_C	H_D	H_E	H_F	H_G	C1/C2	C3/C4	C5/C6	Distortion[a,b]
2NIA	6.32	2.70	2.02	2.00	1.70	54.0	29.2	25.5	0[c]
2NDI	5.59	2.69	2.32	2.04	1.72	57.1	30.8	26.1	13.1
3NDI	6.23	2.48	1.99	1.94	1.67	54.0	30.1	25.9	1.0
4NDI	6.40	2.34	1.88	1.85	1.63	54.9	30.6	25.7	3.1

[a] The distortion on the cyclohexane chair is expressed as sum of the square of the deviation of the chemical shifts with respect to those for **2NIA**. [b] To a first approximation the distortion can be correlated with the relative strain energy computed by DFT methods (RB3LYP/6-31G**). See Figure S24. [c] By definition.

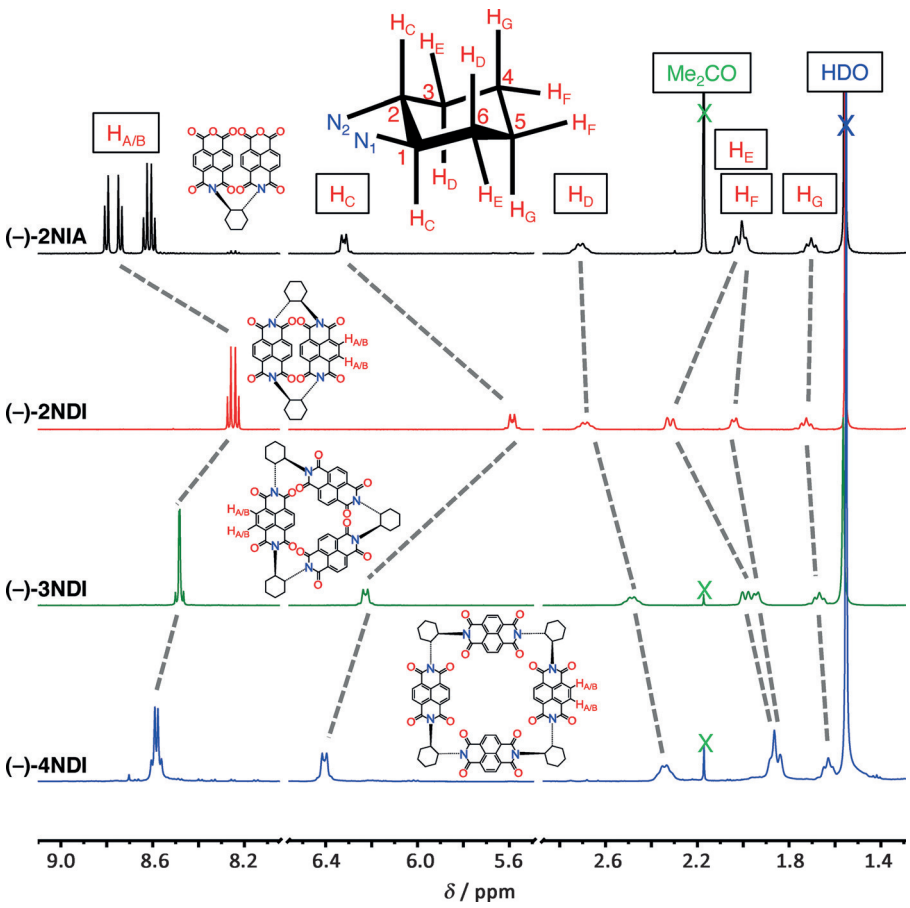

Figure 1. A comparison of the ^{1}H NMR spectra (500 MHz, $CDCl_3$, 298 K) of (−)-**2NIA**, (−)-**2NDI**, (−)-**3NDI**, and (−)-**4NDI**.

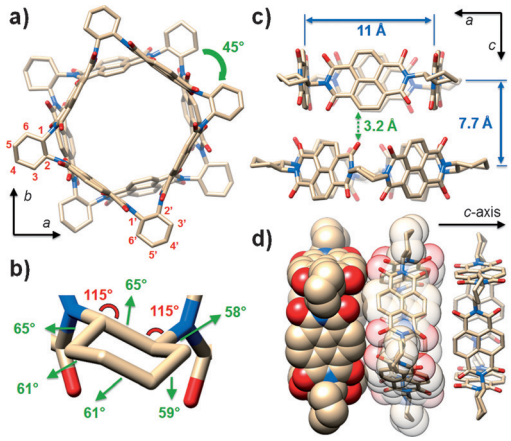

Figure 2. a) Top view of a tubular representation of the crystal structure of molecular square (+)-**4NDI**, showing the nanometer-sized cavity. The hydrogen atoms are omitted for the sake of clarity. b) Expanded view of the cyclohexane skeleton. c) Side-on view showing the supramolecular dimer of two crystallographically distinct (+)-**4NDI** molecules held together by means of multiple intermolecular CH···O hydrogen bonds. Bond angles are shown in red and torsional angles in green. d) A blend of tubular and space-filling representations of the solid-state superstructures of (+)-**4NDI** showing the tubular alignment along the *c*-axis.

respectively) in ***n*NDI**, where $n = 2$ and 3, with respect to those of monomeric **Ref-NDI**, as a consequence of interchromophoric exciton coupling between neighboring NDI units.[19] The $A^{0\leftarrow0}/A^{0\leftarrow1}$ ratio for these vibronic bands increases as the distance between the electronic transition moments, which lie parallel to the long axis of each NDI unit, becomes larger, in good agreement with the excitonic model developed by Kasha.[19] The chiroptical activities in ***n*NDI** are indicated by the strong signal in the electronic circular dichroism (CD) spectra (Figure 3b), which display several sets of degenerate exciton-type Cotton effects. The sign and intensity of these CD bands are correlated with the distance between the NDI chromophores and the dihedral angle between their electronic transition dipoles.[17] In particular, the negative Cotton effect at around 380 nm of (−)-***n*NDI**, which is obtained from (*R*,*R*)-*trans*-1,2-cyclohexanediamine, reflects the negative gauche torsional angle of the N1-C1-C2-N2 bond system of the cyclohexane skeleton. The unsymmetrical shape of the CD band at 380 nm can be explained by the effect of cancellation by the closely lying CD band at 360 nm.

The excited state dynamics of this series of cyclic diimide molecules in CH_2Cl_2 were followed using femtosecond Vis/NIR transient absorption spectroscopy (fsTA). The cyclic tetramer **4NDI** and trimer **3NDI** show (Figure 3c) similar behavior to that of the monomeric **Ref-NDI**. FsTA spectra, following excitation with a 350 nm laser pulse, reveal formation of ^{1}*NDI in all three molecules within the instrument response time (< 200 fs). Global target analysis of the three-dimensional ΔA versus time and wavelength dataset reveals (Figures S9–S12) species-associated differential spectra that indicate the formation of short-lived ^{1}*NDI states (1.2 ± 0.1, 2.5 ± 0.1 and 2.0 ± 0.1 ps for **Ref-NDI**, **3NDI**, and **4NDI**, respectively), which absorb at 606, 730, and 1135 nm, followed by relaxation and fast intersystem crossing to long-lived ^{3}*NDI states, which absorb at 460 and 488 nm.[20] The triplet state decays were followed by nanosecond transient absorption (nsTA, Figures S16–S18). Remarkably, we observed a time-dependent reversal of the intensities of the two peaks of the triplet transient absorption spectrum on the nanosecond timescale for **3NDI** (12.6 ± 0.6 ns) and **4NDI** (19.4 ± 0.3 ns), an observation which is not present in the case of the monomeric **Ref-NDI**. These spectral changes could be indicative of the relaxation of a delocalized triplet exciton to a more localized monomer-like triplet excited state, perhaps

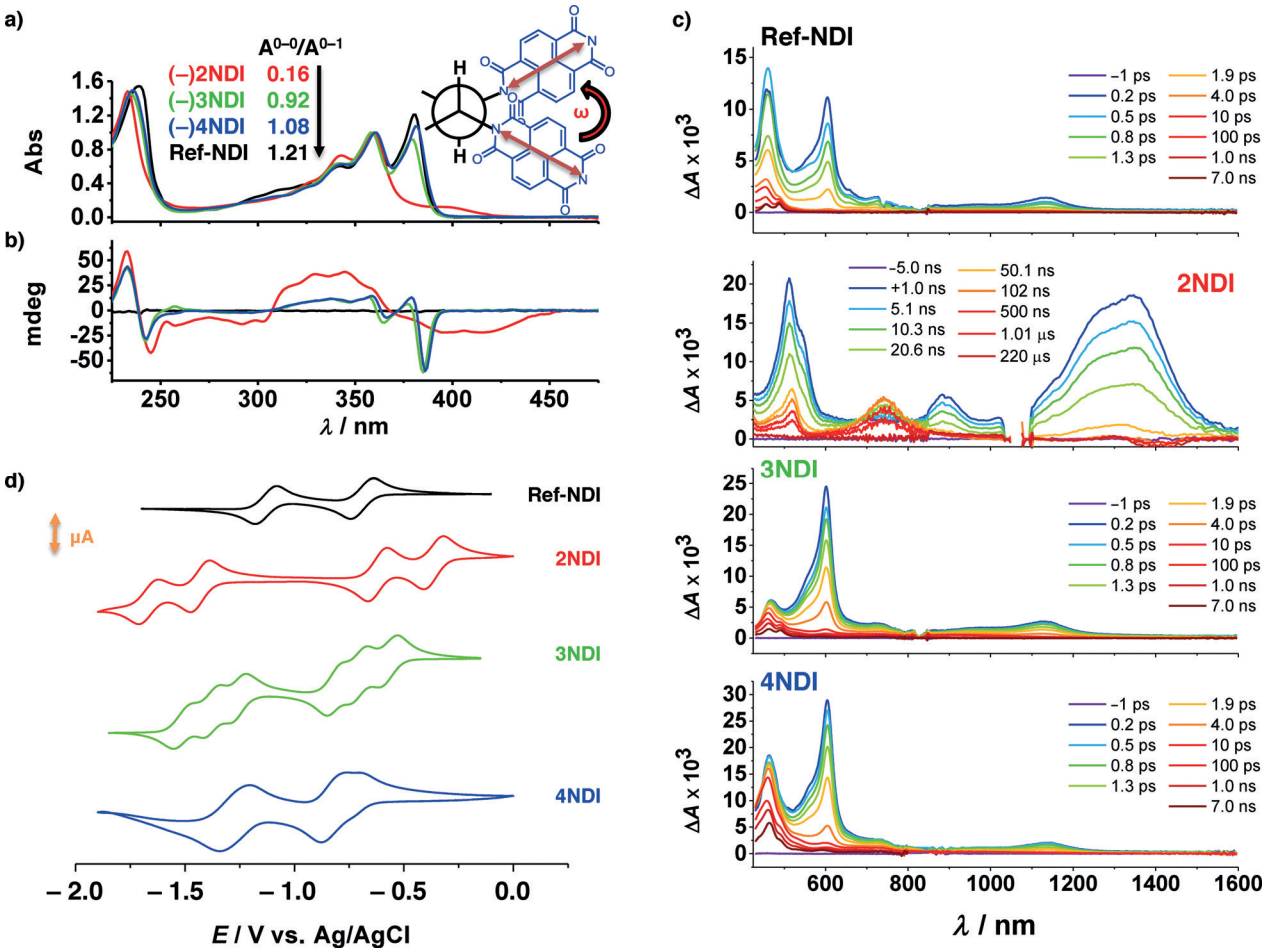

Figure 3. a) UV/Vis absorption and b) CD spectra of (−)-**2NDI** (red traces), (−)-**3NDI** (green traces), and (−)-**4NDI** (blue traces) in CH_2Cl_2 compared with the absorption and CD spectra of the **Ref-NDI** (black traces). (T = 298 K and the concentration was adjusted in order to have the absorbance equal 1.0 at 360 nm.) c) Combined visible and near-infrared femtosecond transient absorption spectra of **Ref-NDI**, (−)-**2NDI**, (−)-**3NDI**, and (−)-**4NDI** in CH_2Cl_2 at 298 K following excitation with a 350 nm laser pulse (0.6 µJ/pulse). d) Cyclic voltammograms (0.5 mM in CH_2Cl_2, 100 mM $TBAPF_6$, 50 mVs^{-1}, 298 K) of **Ref-NDI** (black trace), (−)-**2NDI** (red trace), (−)-**3NDI** (green trace) and (−)-**4NDI** (blue trace). The (+)-***n*NDI** analogues shows identical results except for CD spectra, which display similar Cotton effects, but with inverted signs.

accompanied by a geometrical change. The triplet nature of the latter long-lived excited states is also supported by time-resolved photoluminescence (TRPL) spectroscopy (Figures S19–S21) and time-resolved EPR (TREPR) spectroscopy (Figure S22) at 77 K, which reveal phosphorescence and triplet EPR spectra for all three compounds, similar to those reported[21] for the NDI triplet state. Conversely, the cofacially π-stacked **2NDI** displays ultrafast formation of an excimer-like state, characterized (Figure 3c) by the appearance[22] of a red-shifted transient absorption in the NIR within the instrument response time.[23]

The reduction potentials for this series of macrocyclic NDI molecules are summarized in Table S1 and their cyclic voltammograms (CVs) are presented in Figure 3d. The CVs of **2NDI** and **3NDI** show a clear splitting of the reduction waves into distinct reversible one-electron processes as a consequence of strong electronic coupling. On the other hand, the CV of the tetrameric **4NDI** is more complex and less well-resolved. The differential pulse voltammogram (DPV, Figure S24) along with the CV shows that the first reduction at around −0.71 V generates a distinct, singly reduced [**4NDI**]$^{\cdot-}$ radical anion closely followed by 1) a three-electron reduction process at around −0.85 V and 2) a broad four-electron reduction wave at −1.32 V. This observation is particularly striking as it suggests that, despite the electronic communication between the NDI units, multielectron reduction of **4NDI** only requires a minimal Coulombic energy penalty, which makes this nanometer-sized square an appealing all-organic multielectron acceptor (up to eight electrons) for potential use in artificial photosynthesis and molecular supercapacitors. Upon the partial reduction of **Ref-NDI**, **2NDI**, **3NDI**, and **4NDI** with one equivalent of cobaltocene as a chemical reductant, the stable monoradical anion, as monitored by UV/Vis/NIR absorption (Figure S25), was generated in quantitative yield and subjected to further EPR spectroscopic studies.

The EPR spectra of [**Ref-NDI**]$^{\cdot-}$, [**2NDI**]$^{\cdot-}$, [**3NDI**]$^{\cdot-}$, and [**4NDI**]$^{\cdot-}$ and their corresponding simulations are shown in Figure 4a. If the electron is shared equally within the macrocycles, it is expected from the McConnell relationship[24] that the isotropic hyperfine couplings should decrease linearly with the number of NDI subunits present. In order to

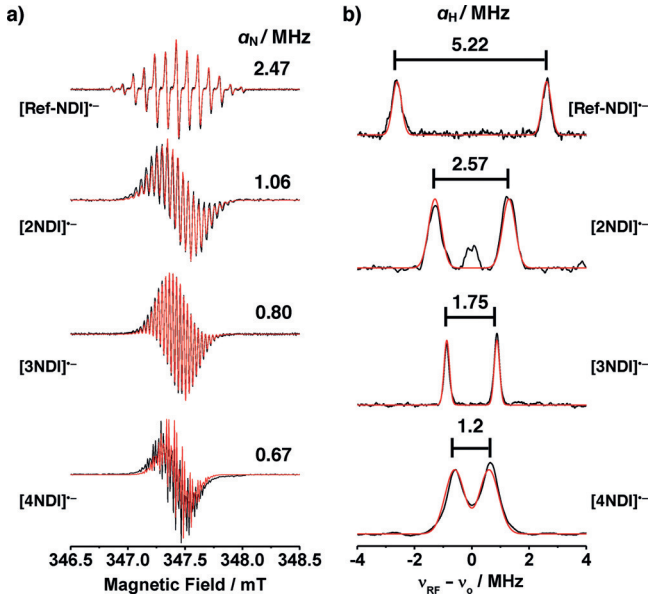

Figure 4. a) CW-EPR spectra and b) ^{1}H ENDOR spectra of [**Ref-NDI**]$^{\bullet-}$, [(−)-**2 NDI**]$^{\bullet-}$, [(−)-**3 NDI**]$^{\bullet-}$ and [(−)-**4 NDI**]$^{\bullet-}$ produced by monoreduction of neutral states with 1 equiv of cobaltocene. Overlay between the experimental spectra (black traces, 0.25 mM in CH_2Cl_2, 298 K) and their simulated spectra (red traces). Isotropic nitrogen and proton hyperfine coupling constants are obtained from CW-EPR and ^{1}H ENDOR, respectively.

measure the isotropic hydrogen hyperfine coupling, a_H, more accurately, continuous-wave ENDOR[25] was also performed (Figure 4b). The results from fitting the ENDOR spectra show an n-fold reduction of a_H for the [***n*NDI**]$^{\bullet-}$ radical anions relative to those of [**Ref-NDI**]$^{\bullet-}$, consistent with electron sharing among n NDI units.[26] The reason for such efficient electron sharing could be a consequence of the perfect match of LUMOs associated with the NDI units in the macrocycles which have much higher symmetry than the π-stacked or linear arrays.

In summary, we have prepared a shape-persistent chiral molecular square **4NDI** using a stepwise approach from readily available starting materials. We have observed strong bisignate Cotton effects whose sign supports the absolute configuration of the compound. The solid-state X-ray diffraction analysis of single crystals corroborates the conformational information obtained from spectroscopic studies and reveals a remarkably well-aligned tubular superstructure, sustained by intermolecular hydrogen bonding interactions. We envision that the strong induced chiroptical activity combined with the accessible cavity of **4NDI** could be potentially used for enantioselective recognition, sensing and catalysis. Moreover, electronic spectroscopies and cyclic voltammetry of these structurally well-defined ***n*NDI** polygons show that the strength of the excitonic-coupling and electronic communication between the neighboring NDI units is highly dependent on their separations and relative orientations, affecting the through-space dipole–dipole interaction and interchromophoric orbital overlap. The EPR/ENDOR investigations indicate that the unpaired electron in the monoreduced mixed-valence oxidation state, namely ***n*NDI**$^{\bullet-}$, is fully shared among all n NDI-based redox sites, suggesting that the electron migration rate in ***n*NDI**$^{\bullet-}$ is faster than the timescale ($>10^7\,s^{-1}$) of the EPR/ENDOR experiments, even when the angle between the π systems approaches orthogonality and the orbital overlap is minimal, as in **4NDI**. These results also suggest that a fast hopping mechanism may underlie the efficient electron sharing within the cyclic NDI oligomers linked by rigid vicinal diamine linkers. The potential of shape-persistent diimide macrocycles to carry out long-distance electron transport required for organic electronics and photovoltaics applications is apparent.

Acknowledgements

We thank Dr. Saman Shafaie for collecting high-resolution mass spectrometric data, Dr. Amy A. Sarjeant for solving the single crystal X-ray structures, and Rufei Shi for helpful discussions. This research was supported by the Chemical Sciences, Geosciences, and Biosciences Division, Office of Basic Energy Sciences, DOE, under grant no. DE-FG02-99ER14999 (M.R.W.) and is also part (Project 32-949) of the Joint Center of Excellence in Integrated Nano-Systems (JCIN) at King Abdulaziz City for Science and Technology (KACST) and Northwestern University (NU). The authors would like to thank both KACST and NU for their continued support of this research. R.M.Y. was supported as part of the ANSER Center, an Energy Frontier Research Center funded by the U.S. Department of Energy (DOE), Office of Science, Basic Energy Sciences (BES), under Award #DE-SC0001059 (fsTA experiments). Y.W. thanks the Fulbright Scholars Program for a Graduate Research Fellowship and also gratefully acknowledges support of a Ryan Fellowship from the NU International Institute for Nanotechnology (IIN).

Keywords: electron transport · hydrogen bonding · molecular squares · molecular electronics · organic semiconductors

How to cite: *Angew. Chem. Int. Ed.* **2015**, *54*, 11971–11977
Angew. Chem. **2015**, *127*, 12139–12145

[1] X. G. Guo, A. Facchetti, T. J. Marks, *Chem. Rev.* **2014**, *114*, 8943–9021.
[2] a) M. R. Wasielewski, *Acc. Chem. Res.* **2009**, *42*, 1910–1921; b) T. M. Wilson, T. A. Zeidan, M. Hariharan, F. D. Lewis, M. R. Wasielewski, *Angew. Chem. Int. Ed.* **2010**, *49*, 2385–2388; *Angew. Chem.* **2010**, *122*, 2435–2438.
[3] a) K. Susumu, P. R. Frail, P. J. Angiolillo, M. J. Therien, *J. Am. Chem. Soc.* **2006**, *128*, 8380–8381; b) V. Lloveras, J. Vidal-Gancedo, T. M. Figueira-Duarte, J. F. Nierengarten, J. J. Novoa, F. Mota, N. Ventosa, C. Rovira, J. Veciana, *J. Am. Chem. Soc.* **2011**, *133*, 5818–5833; c) M. Gilbert Gatty, A. Kahnt, L. J. Esdaile, M. Hutin, H. L. Anderson, B. Albinsson, *J. Phys. Chem. B* **2015**, *119*, 7598–7611.
[4] For reviews on NDI, see: a) S. V. Bhosale, C. H. Jani, S. J. Langford, *Chem. Soc. Rev.* **2008**, *37*, 331–342; b) S. L. Suraru, F. Würthner, *Angew. Chem. Int. Ed.* **2014**, *53*, 7428–7448; *Angew. Chem.* **2014**, *126*, 7558–7578.

[5] a) X. W. Zhan, A. Facchetti, S. Barlow, T. J. Marks, M. A. Ratner, M. R. Wasielewski, S. R. Marder, *Adv. Mater.* **2011**, *23*, 268 – 284; b) T. He, M. Stolte, F. Würthner, *Adv. Mater.* **2013**, *25*, 6951 – 6955.

[6] H. Huang, N. J. Zhou, R. P. Ortiz, Z. H. Chen, S. Loser, S. M. Zhang, X. G. Guo, J. Casado, J. T. L. Navarrete, X. G. Yu, A. Facchetti, T. J. Marks, *Adv. Funct. Mater.* **2014**, *24*, 2782 – 2793.

[7] a) Z. X. Zhu, C. J. Cardin, Y. Gan, H. M. Colquhoun, *Nat. Chem.* **2010**, *2*, 653 – 660; b) N. Ponnuswamy, G. D. Pantos, M. M. J. Smulders, J. K. M. Sanders, *J. Am. Chem. Soc.* **2012**, *134*, 566 – 573; c) G. Sforazzini, E. Orentas, A. Bolag, N. Sakai, S. Matile, *J. Am. Chem. Soc.* **2013**, *135*, 12082 – 12090; d) S. K. M. Nalluri, C. Berdugo, N. Javid, P. W. J. M. Frederix, R. V. Ulijn, *Angew. Chem. Int. Ed.* **2014**, *53*, 5882 – 5887; *Angew. Chem.* **2014**, *126*, 5992 – 5997; e) A. Das, S. Ghosh, *Angew. Chem. Int. Ed.* **2014**, *53*, 1092 – 1097; *Angew. Chem.* **2014**, *126*, 1110 – 1115.

[8] a) M. Borgström, N. Shaikh, O. Johansson, M. F. Anderlund, S. Styring, B. Åkermark, A. Magnuson, L. Hammarström, *J. Am. Chem. Soc.* **2005**, *127*, 17504 – 17515; b) S. Bhosale, A. L. Sisson, P. Talukdar, A. Furstenberg, N. Banerji, E. Vauthey, G. Bollot, J. Mareda, C. Roger, F. Würthner, N. Sakai, S. Matile, *Science* **2006**, *313*, 84 – 86; c) E. Iengo, G. D. Pantoş, J. K. M. Sanders, M. Orlandi, C. Chiorboli, S. Fracasso, F. Scandola, *Chem. Sci.* **2011**, *2*, 676 – 685; d) Y. Matsunaga, K. Goto, K. Kubono, K. Sako, T. Shinmyozu, *Chem. Eur. J.* **2014**, *20*, 7309 – 7316.

[9] Y. J. Zhao, N. Sakai, S. Matile, *Nat. Commun.* **2014**, *5*, 3911.

[10] a) S. T. Schneebeli, M. Frasconi, Z. C. Liu, Y. L. Wu, D. M. Gardner, N. L. Strutt, C. Y. Cheng, R. Carmieli, M. R. Wasielewski, J. F. Stoddart, *Angew. Chem. Int. Ed.* **2013**, *52*, 13100 – 13104; *Angew. Chem.* **2013**, *125*, 13338 – 13342; b) Y. L. Wu, M. Frasconi, D. M. Gardner, P. R. McGonigal, S. T. Schneebeli, M. R. Wasielewski, J. F. Stoddart, *Angew. Chem. Int. Ed.* **2014**, *53*, 9476 – 9481; *Angew. Chem.* **2014**, *126*, 9630 – 9635.

[11] For reviews on shape-persistent macrocycles, see: a) S. Höger, *J. Polym. Sci. Part A* **1999**, *37*, 2685 – 2698; b) C. Grave, A. D. Schlüter, *Eur. J. Org. Chem.* **2002**, 3075 – 3098; c) D. Zhao, J. S. Moore, *Chem. Commun.* **2003**, 807 – 818; d) M. Iyoda, J. Yamakawa, M. J. Rahman, *Angew. Chem. Int. Ed.* **2011**, *50*, 10522 – 10553; *Angew. Chem.* **2011**, *123*, 10708 – 10740.

[12] It is worth mentioning that while the metallomacrocyclic molecular squares have become easily accessible, thanks to the metal-directed self-assembly approaches, covalent molecular squares still remain rare on account of the synthetic challenges they pose. For examples of metallocyclic squares and their applications, see: a) M. Fujita, J. Yazaki, K. Ogura, *J. Am. Chem. Soc.* **1990**, *112*, 5645 – 5647; b) P. J. Stang, B. Olenyuk, *Acc. Chem. Res.* **1997**, *30*, 502 – 518; c) S. J. Lee, W. B. Lin, *J. Am. Chem. Soc.* **2002**, *124*, 4554 – 4555; d) F. Würthner, C.-C. You, C. R. Saha-Möller, *Chem. Soc. Rev.* **2004**, *33*, 133 – 146.

[13] For other examples of preparation of NDI macrocycles using the protection group strategy, see: a) S. Gabutti, M. Knutzen, M. Neuburger, G. Schull, R. Berndt, M. Mayor, *Chem. Commun.* **2008**, 2370 – 2372; b) S. Gabutti, S. Schaffner, M. Neuburger, M. Fischer, G. Schafer, M. Mayor, *Org. Biomol. Chem.* **2009**, *7*, 3222 – 3229.

[14] This decrease of the shielding effect on the protons by adjacent NDI π systems correlates with the NDI–NDI distance, which becomes larger as *n* increases. Moreover, the aliphatic protons of the cyclohexane rings display the characteristic pattern of ^{1}H NMR resonances of a "locked" chair conformation with vicinal axial-axial ($^3J_{a-a} = 10$–12 Hz) and axial-equatorial ($^3J_{a-e} =$ 3–4 Hz) coupling constants, which confirms the diequatorial conformation for the imide substituents. Although the spectra are not resolved well enough to permit an accurate determination of *J* values, the pronounced differences in chemical shifts of the cyclohexane protons suggest a substantial distortion of its skeleton in the three NDI polygons compared to an open-chain dimer (Figure 1), which contains a relatively distortion-free cyclohexane chair with vicinal imide substituents (**2NIA**). The sum of the squares of the deviation in chemical shifts for the cyclohexane protons/carbons resonances shows (Table 1) a three-fold increase in **4NDI** compared to **3NDI** and becomes severe (ca. 13-fold) in the dimer. The 2D diffusion ordered ^{1}H NMR (DOSY; Figure S5) of ***n*NDI** was also performed and shows a clear decrease in diffusion constants ($D = 7.9\ m^2 s^{-1}$ for **2NDI**, $5.7\ m^2 s^{-1}$ for **3NDI** and $5.0\ m^2 s^{-1}$ for **4NDI**) in line with increasing molecular radii for this series of NDI polygons.

[15] Crystallographic data for $C_{80}H_{56}N_8O_{16}$ ($M = 1385.32$): orthorhombic, space group $P2_12_12$ (no. 18), $a = 21.680(2)$, $b = 30.545(5)$, $c = 15.5369(18)$ Å, $V = 10289(2)$ Å^3, $Z = 4$, $T = 100.0$ K, μ(CuKα) $= 0.524\ mm^{-1}$, $D_{calc} = 0.894\ g\,m^{-1}\,m^3$, 17214 reflections measured ($5.69 \le 2\theta \le 88.98$), 7980 unique ($R_{int} = 0.0929$, $R_{sigma} = 0.1715$) which were used in all calculations. The final R_1 was 0.0552 ($I > 2\sigma(I)$) and wR_2 was 0.1120 (all data). CCDC 1041583 contains the supplementary crystallographic data for this paper. These data can be obtained free of charge from The Cambridge Crystallographic Data Centre.

[16] With a size comparable to three π–π stacking distances, **4NDI** can potentially encapsulate two aromatic guests, such as benzene, pyrene, or naphthalene derivatives, by means of aromatic charge-transfer or π-stacking interactions.

[17] a) J. Gawroński, F. Kazmierczak, K. Gawrońska, U. Rychlewska, B. Norden, A. Holmen, *J. Am. Chem. Soc.* **1998**, *120*, 12083 – 12091; b) J. Gawroński, M. Brzostowska, K. Kacprzak, H. Kołbon, P. Skowronek, *Chirality* **2000**, *12*, 263 – 268; c) J. Gawroński, M. Brzostowska, K. Gawrońska, J. Koput, U. Rychlewska, P. Skowronek, B. Nordén, *Chem. Eur. J.* **2002**, *8*, 2484 – 2494.

[18] The bending of the aromatic systems, such as those found in cycloparaphenylene, is of considerable interest, not only because of synthetic challenge and aesthetic beauty, but also because of the desire to understand how the strain can be tapped to affect device performance. For recent examples, see: a) R. Jasti, J. Bhattacharjee, J. B. Neaton, C. R. Bertozzi, *J. Am. Chem. Soc.* **2008**, *130*, 17646 – 17647; b) B. L. Merner, L. N. Dawe, G. J. Bodwell, *Angew. Chem. Int. Ed.* **2009**, *48*, 5487 – 5491; *Angew. Chem.* **2009**, *121*, 5595 – 5599; c) H. Takaba, H. Omachi, Y. Yamamoto, J. Bouffard, K. Itami, *Angew. Chem. Int. Ed.* **2009**, *48*, 6112 – 6116; *Angew. Chem.* **2009**, *121*, 6228 – 6232; d) S. Yamago, Y. Watanabe, T. Iwamoto, *Angew. Chem. Int. Ed.* **2010**, *49*, 757 – 759; *Angew. Chem.* **2010**, *122*, 769 – 771; e) Y. Koyama, S. Hiroto, H. Shinokubo, *Angew. Chem. Int. Ed.* **2013**, *52*, 5740 – 5743; *Angew. Chem.* **2013**, *125*, 5852 – 5855; f) P. J. Evans, E. R. Darzi, R. Jasti, *Nat. Chem.* **2014**, *6*, 404 – 408. For a review of cylophane chemistry, see: *Modern Cyclophane Chemistry* (Eds.: R. Gleiter, H. Hopf), Wiley-VCH, Weinheim, **2004**.

[19] M. Kasha, H. R. Rawles, M. L. El-Bayoumi, *Pure Appl. Chem.* **1965**, *11*, 371 – 392.

[20] The observed extension of the singlet-excited-state lifetime can be attributed to the decrease of nonradiative rate constants in the rigid macrocycles, where some of vibrational modes, needed for either ISC or internal conversion, are more restricted.

[21] G. P. Wiederrecht, W. A. Svec, M. R. Wasielewski, T. Galili, H. Levanon, *J. Am. Chem. Soc.* **2000**, *122*, 9715 – 9722.

[22] For NIR absorption of aromatic excimers, see, for example: a) R. Katoh, E. Katoh, N. Nakashima, M. Yuuki, M. Kotani, *J. Phys. Chem. A* **1997**, *101*, 7725 – 7728; b) K. E. Brown, W. A. Salamant, L. E. Shoer, R. M. Young, M. R. Wasielewski, *J. Phys. Chem. Lett.* **2014**, *5*, 2588 – 2593.

[23] This excimer-like state decays within 21 ns into a long-lived triplet state, which has very different TA (Figures S13 – S15) and EPR spectra (Figure S18) with respect to the monomeric **Ref-NDI** because of the strong electronic coupling between the two NDI subunits. In particular, the TA spectrum of the excited

triplet state of **2NDI** is considerably red-shifted (750 nm) compared to that (488 nm) of the **Ref-NDI**. The triplet EPR spectrum of **2NDI** is also narrowed. Fitting a simulation to the signal (Figure S21) gave zero-field splitting parameters of $|D| = 607$ and $E/D = 0.0132$ (units of 10^{-4} cm^{-1}). In contrast, zero-field splitting parameters for typical NDI monomers have been reported[20] as $|D| = 743$ and $E/D = 0.0162$. These results may indicate that a charge transfer configuration, in which the two unpaired electrons constituting the triplet state each reside on adjacent NDI molecules, contributes to the overall triplet wavefunction. See: M. C. Thurnauer, J. J. Katz, J. R. Norris, *Proc. Natl. Acad. Sci. USA* **1975**, *72*, 3270 – 3274.

[24] a) H. M. McConnell, *J. Chem. Phys.* **1956**, *24*, 632 – 632; b) H. M. McConnell, *J. Chem. Phys.* **1956**, *24*, 764 – 766; c) J. R. Norris, R. A. Uphaus, H. L. Crespi, J. Katz, *Proc. Natl. Acad. Sci. USA* **1971**, *68*, 625 – 628.

[25] ENDOR spectroscopy of the radical anions was performed in CH_2Cl_2 solution using the resonance condition $\nu^{\pm} = |\nu_n \pm a_{H/2}|$, in which $\nu^{\pm}$ is the ENDOR transition frequency and ν_n is the proton Larmor frequency. For more details, see, for example: H. Kurreck, B. Kirste, W. Lubitz, *Electron Nuclear Double Resonance Spectroscopy of Radicals in Solution*, VCH, Weinheim, **1988**.

[26] The nitrogen isotropic hyperfine interaction, a_N, was obtained through simulation of the cw-EPR spectra by keeping a_H fixed to the values obtained from ENDOR.

Received: May 26, 2015
Published online: August 20, 2015

